IEEE Photonics Journal
An IEEE Photonics Society Publication

Open Access

Distributed Fiber Voice Sensor Based on Phase-Sensitive Optical Time-Domain Reflectometry

Volume 7, Number 6, December 2015

Yuqing Wu
Jiulin Gan
Qingyu Li
Zhishen Zhang
Xiaobo Heng
Zhongmin Yang

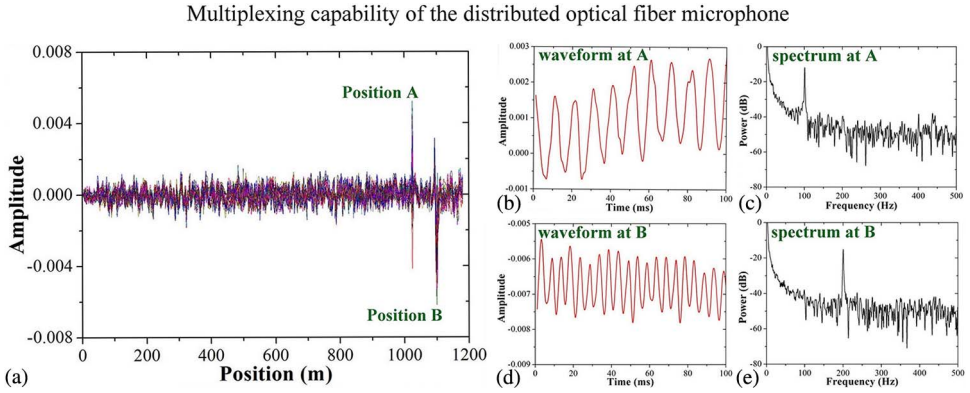

DOI: 10.1109/JPHOT.2015.2499539
1943-0655

Distributed Fiber Voice Sensor Based on Phase-Sensitive Optical Time-Domain Reflectometry

Yuqing Wu,[1,2] Jiulin Gan,[1,2] Qingyu Li,[1,2] Zhishen Zhang,[1,2] Xiaobo Heng,[1,2] and Zhongmin Yang[1,2]

[1]State Key Laboratory of Luminescent Materials and Devices, South China University of Technology, Guangzhou 510640, China
[2]Special Glass Fiber and Device Engineering Technology Research and Development Center of Guangdong Province, Guangzhou 510640, China

DOI: 10.1109/JPHOT.2015.2499539

Manuscript received October 13, 2015; accepted November 6, 2015. Date of publication November 10, 2015; date of current version November 19, 2015. This work was supported in part by the China State 863 Hi-tech Program under Grant 2012AA041203, by the National Natural Science Foundation of China under Grant 61575064, by the Fundamental Research Funds for the Central Universities under Grant 2014ZM0033, and by the National Science Fund for Distinguished Young Scholars of China under Grant 61325024. Corresponding author: J. Gan (e-mail: msgan@scut.edu.cn).

Abstract: A fiber-optic phase-sensitive optical time-domain reflectometry (φ-OTDR) distributed sensing system has been proposed and demonstrated for human-voice detecting and reproducing applications. The fiber strain induced by the voice is ultra small (just a few nε); thus, the change of related Rayleigh backscattering light intensity and phase are much too small for effective detection based on the conventional fiber φ-OTDR system. Utilizing the flat-packaged fiber design, the strengthened φ-OTDR system shows better performance with higher signal-to-noise ratio (SNR) up to 35 dB. The audio frequency and amplitude response have been investigated. The multiplexing capability of this distributed optical fiber microphone also has been proved with 1.2-km sensing range and 5-m spatial resolution.

Index Terms: Fiber optics sensors, remote sensing and sensors, Rayleigh scattering.

1. Introduction

Acoustic sound can be detected by using an optical fiber sensor since the original demonstration by Cole *et al.* [1] and Bucaro *et al.* [2]. Compared with the conventional electronic microphone, fiber-optic acoustic sensors have the advantages of large bandwidth, immunity to electromagnetic and radio frequency interference, remote sensing capability, direct connection to the optical transmission network, and so on [3], [4]. There has been a great deal of research in the last three decades contributing to the development of fiber-optic acoustic sensors and related technologies, such as FP/MZ interferometers [5], [6], fiber Bragg grating (FBG) [7], DFB/DBR lasers [8]–[10], etc. However, these point/multipoint acoustic detecting schemes are often not easy to achieve large-scale multiplexing and distributed sensing.

The acoustic wave will induce a non-direct-contact stress on the sensing fiber at close range through air/water vibration pressure, and the induced strain of disturbed fiber is very slight (just a few nε), so the acoustic wave fiber sensing is essentially the dynamic strain measurement with high frequency response and ultrahigh sensitivity. The long-distance distributed dynamic

large strain optical fiber sensor has been most extensively explored using coherent Rayleigh scattering [11]–[20], and a number of commercial devices are capable of detecting multiple strain perturbations and positioning disturbed locations.

Long-distance, high-frequency response and accurate measurement are the three potential advantages of the distributed optical-fiber φ-OTDR system. Until now, the detecting-distance is longer than 100 km by utilizing the distributed fiber Raman or Brillouin amplification [11]–[13]. φ-OTDR with kHz-scale frequency response has been demonstrated by balancing the sensing range and pulse repetition rate [14], [15]. Combined with frequency-division multiplexing [16], [17] or Mach–Zehnder interferometer [18], φ-OTDR with frequency response up to MHz level has also been proposed and achieved. Most of the φ-OTDR researches focus on differential Rayleigh scattering interferometric amplitude traces detection principle [11]–[18], which reveals vibration with acceptable accuracy. Meanwhile, a few work concentrates on obtaining the interferometric phase information. The phase change is considered as the direct response to the external vibration information [19], [20]. The interferometric phase information can reflect the disturbance information more accurately, but the phase continuous cumulative effect and phase unwrap technical problem restrict the further application.

Compared with the acoustic wave detection, the above researches have focused on the relatively large strain measurement, and the first distributed acoustic optical fiber sensor was conceptual introduced by utilizing coherent backward Rayleigh scattering light [21]. After that, just a few studies concentrate on improving the sensitivity of the φ-OTDR system for the weak acoustic wave detection [22]–[24]. Masoudi *et al.* demonstrated 80 nε minimum detectable strain perturbation of the φ-OTDR system using a 3 $\times$ 3 coupler MZI for demodulation [23]. Rao *et al.* proposed sound over fiber communication scheme based on φ-OTDR system [24]. However, it still needs to further improve the sensitivity for practical distributed optical fiber microphone application, and a fully detailed and complete demonstration has not been executed and reported.

When the acoustic wave propagates in the air/water and meets the fiber exposed to its filed, a very small part of acoustic pressure will exert on the fiber and induce fiber strain. The frequency and amplitude of the dynamic fiber strain are related with the acoustic characteristic parameters. Aimed at the human voice detecting and reproducing application, where the frequency range is mainly about 65 Hz–1100 Hz, the conventional φ-OTDR system is theoretically qualified for the requirement of this frequency response range. However, the relatively low sensitivity of voice detecting based on φ-OTDR system is the biggest technical obstacle for the practical application. Here, in this paper, the flat-packaged fiber structure is designed and applied as the sensing element, which can absorb and transfer more acoustic energy to the fiber. A narrow linewidth fiber laser and heterodyne coherent detection have been used to improve the signal-to-noise ratio of the system; interferometric amplitude difference information has been acquired and analyzed for acoustic wave demodulation with a relatively high SNR. Based on this flat-packaged amplitude demodulated φ-OTDR system, the frequency response and sensitivity have been investigated, and the multiplexing capability of this distributed optical fiber microphone have been proved. The demonstration of human voice detection and reproduction are also illustrated.

2. Experimental Setup and Results

When an optical pulse is injected into the fiber, it will scatter light along almost all directions based on Rayleigh scattering effect. But only the Rayleigh backscattering power can propagate in fiber and be captured as shown in Fig. 1(a), which can be derived as follows [24]:

$$P_{rs}(z) = P_0\left(\frac{V_g T}{2}\right)\alpha_R S \exp(-2\alpha z) \tag{1}$$

where P_{rs} and P_0 are the backscattered power and the input power, respectively. V_g is the group velocity of light. T is temporal width of the optical pulse. α is the total loss of the fiber. α_R is the Rayleigh scattering coefficient and defined by K/λ^4 (where K is a constant, and λ is the

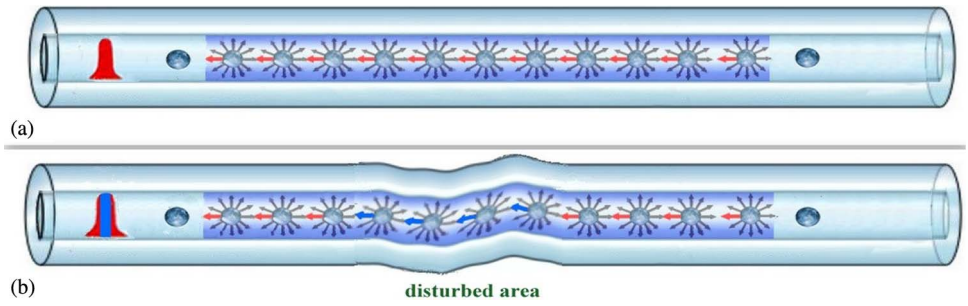

Fig. 1. Rayleigh scattering effect within fiber. (a) Fiber without disturbance. (b) Fiber with local disturbance.

wavelength of the light). α_R is related with the fiber material and injected light wavelength. S is the recapture factor of the fiber and is defined as

$$S = \frac{3/2}{(\omega/r)^2 V^2} \frac{NA^2}{n_1^2} \tag{2}$$

where ω is the spot size of the light beam. r is the core radius. V is the normalized frequency. NA is the numerical aperture $(NA = (n_1^2 - n_2^2)^{1/2})$, and n_1 and n_2 are the refractive indices of the core and the cladding, respectively. From (1), the Rayleigh backscattering power in fiber is directly proportional to the product of α_R and S, and in common single-mode fiber, Rayleigh backscattering coefficient $\alpha_R S$ was estimated and measured to be about –40 dB [24].

Within the fiber range L, the composite reflection is a sum of that from every scatter:

$$E_s(t) = A_0 \sum_{i=1}^{M} a_i \exp(j\phi_i(t)) \tag{3}$$

where M is the amount of backscattering points distributing in section from z to $z + \Delta z$ randomly on the order of $\Delta z/\lambda$, A_0 is the amplitude of the injection light, a_i is the reflectivity of the i_{th} backscattering point along the fiber, and $\phi_i(t)$ is the phase of the i_{th} backscattering point along the fiber.

As illustrated schematically in Fig. 1, based on Rayleigh scattering effect, every point will scatter light along almost all directions, but only the backward scattering light along the injecting light trace can propagate in fiber and be captured. When vibrations are applied on the fiber, the total Rayleigh scattering effect is nearly the same, but the captured backward scattering light will change according to the displacement and deformation of the local scattering point as shown in Fig. 1(b), which means the reflectivity of the scatter point has been modulated by the vibrations. Meanwhile, the vibration-induced strain will also modulate the phase difference of the scattering light.

The composite reflection $E_S(t)$ can be rewritten as

$$E_s(t) = A_0 |r_0 + \Delta r(t)| \exp\, j(\phi_0 + \delta\phi(t)) \tag{4}$$

where r_0 and ϕ_0 are the total equivalent reflectivity and phase without disturbance, respectively; $\Delta r(t)$ and $\delta\phi(t)$ are the relative equivalent reflectivity and phase change under disturbance, respectively. The composite reflection $E_S(t)$ is commonly too weak for direct detection, and the information in $\Delta r(t)$ and $\delta\phi(t)$ can be amplified and acquired by heterodyne detection scheme. The Rayleigh backscattered light E_S is mixed with the local light E_L by a 3 dB coupler. The mixed signal is then launched into a photon detector, and the detected current is proportional to the optical power

$$I(t) \propto E_s^2 + E_L^2 + 2A_0 |r_0 + \Delta r(t)| \times E_L \cos\theta(t) \cos(2\pi(\nu_1 - \nu_0)t + \Delta\phi(t)) \tag{5}$$

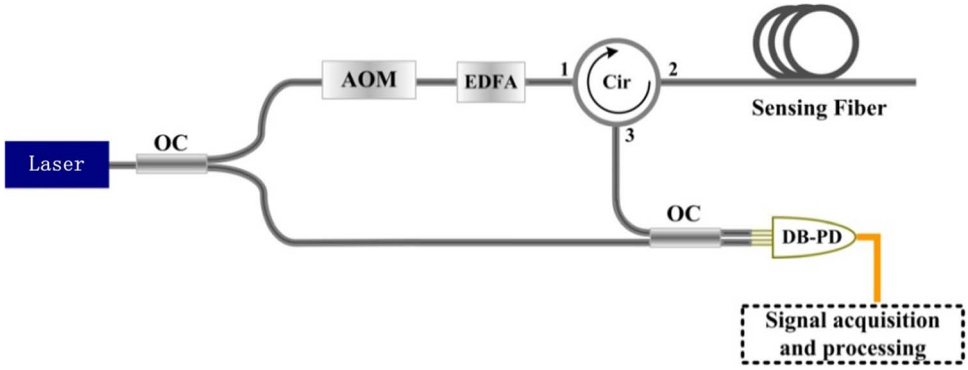

Fig. 2. Experimental setup: OC, optical coupler; AOM, acoustic optical modulator; EDFA, erbium-doped fiber amplifier; Cir, circulator; DB-PD, double balanced photo detector.

where ν_1 and ν_0 are the optical frequency of the signal light and local light, respectively; $\Delta\phi(t) = \phi_0 + \delta\phi(t) - \phi_L$ is the phase difference between E_S and E_L; $\theta(t)$ stands for the polarization deviated from local light, which also varies temporally and spatially.

The beat signal with frequency $\nu_1 - \nu_0$ collected by a photon detector is recorded by a high-speed data acquisition card. By using digital correlation with the beat frequency, two quadrature components of the signal are obtained as functions of time:

$$\begin{aligned} I &\propto A_0 \Delta r(t) \cos\Delta\phi(t) \\ Q &\propto A_0 \Delta r(t) \sin\Delta\phi(t). \end{aligned} \tag{6}$$

The amplitude and phase of backscattering signal can then be obtained as

$$\begin{aligned} \Delta r(t) &\propto \sqrt{I^2 + Q^2} \\ \Delta\phi(t) &\propto \arctan(Q/I) + 2n\pi \end{aligned} \tag{7}$$

where n is an integer.

From (5)–(7), we can see that both the interferometric amplitude and phase difference of backscattering signal can be acquired and obtained for revealing the disturbance information. However, the interferometric phase difference demodulation scheme has two negative factors: First, the phase change of the light in fiber have continuous cumulative effect, which will induce crosstalk at the distributed multiple sensing situation; second, the phase change $\arctan(Q/I)$ exits singularity when component I is very close to 0, and phase-unwrapping technology ($2n\pi$ component) will also induce some errors. Finally, the interferometric amplitude (reflectivity) difference demodulation scheme has been adopted.

The configuration of φ-OTDR system is shown in Fig. 2. The pump laser source is a self-developed 1550 nm single-frequency fiber laser with a 5 kHz linewidth and low intensity noise [26]. The single frequency narrow linewidth laser with 40 mW power output is split into the probe and local paths by a 95/5 optical coupler (OC). The smaller part is acting as local oscillator light, and the main part is pulse modulated by an AOM with pulse width of 50 ns and repetition rate of 10 kHz. The AOM introduces a 160 MHz frequency downshift. The probe pulse is optically amplified by an EDFA and the peak power of the pulse is above 30 dBm. The probe pulse is injected into the sensing fiber (Corning SMF-28) through a circulator. The backscattered Rayleigh signal is combined with the local oscillator light through a 3 dB fiber OC. The beat signal with a frequency about 160 MHz is collected by DB-PD associated with high-speed data acquisition card (DAQ), in which the data-acquisition is synchronous with the signal generator of the AOM. Acquisition and analysis of the sensing signal are real-time processed by a self-designed program.

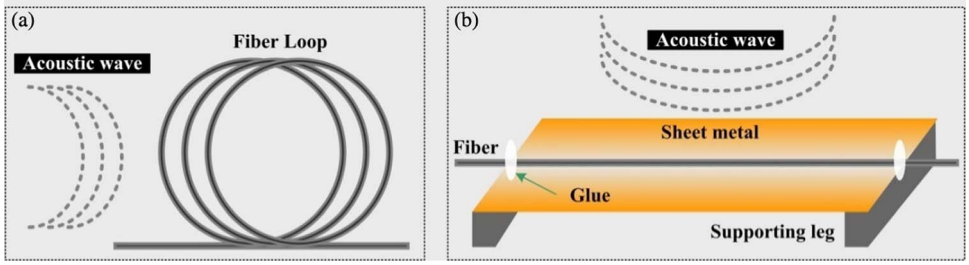

Fig. 3. Fiber acoustic wave sensing reinforcement configuration. (a) Suspend-loop setting. (b) Flat-packaged setting.

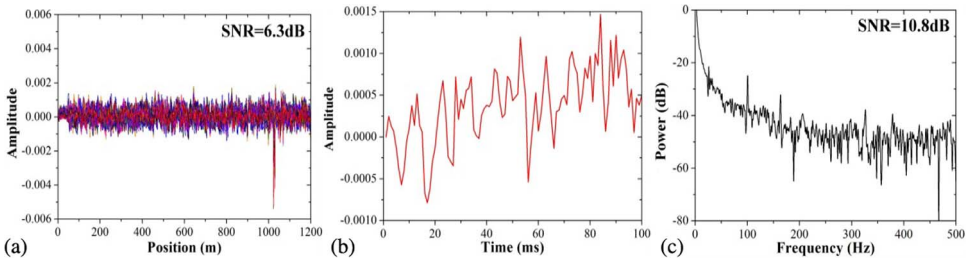

Fig. 4. Experimental result of the acoustic wave response based on the suspend-loop setting. (a) Distributed differential amplitude traces. (b) Differential amplitude time-varying waveforms at the vibration point. (c) Frequency spectrum of the amplitude waveforms.

The Rayleigh backscattering light from the injected pulses is detected and recorded as a function of time. At a single point in time, the received light is the sum of the Rayleigh backscattering light of every scatter point within a fiber section range, which is mainly determined by the pulse width. The spatial resolution L is determined by $L = cT/2n$, where c is the light velocity in vacuum, n is the refractive index of fiber, T is the pulse width. Here, the c, n, and T are set to be 3×10^8 m/s, 1.45, and 50 ns, respectively, so that the spatial resolution in our experiment is 5 m.

The purpose of our experiment focuses on researching the sensor's response to acoustic wave, especially the human voice. By using signal generator, sinusoidal voltages with different frequencies are applied to a loud-speaker for generating sound waves. To monitor the pressure and the frequency of the sound wave applied at the fiber, a calibrated electronic microphone is placed close to the fiber.

As shown in Fig. 3(a), loops fiber with radius of 6 cm is hung 5 cm in front of the loud-speaker without any support, which is located around 1023 m along 1200 m testing fiber. Total length of the loops fiber is about 5 m. 100 Hz sinusoidal voltage has been applied to the loud-speaker, and the sound pressure measured by the electronic microphone is about 85 dBC. Through the signal processing scheme mentioned above, we get the differential amplitude traces as shown in Fig. 4(a), the sound vibration location could be clearly observed at the 1023 m position. Here the global signal-to-noise ratio (SNR) is defined as an amplitude ratio between signal peak amplitude and the background noise level $\mathrm{SNR} = 10\log(V_{\mathrm{signal}}/V_{\mathrm{noise}})$. Based on this suspend-loop setting, the global SNR is 6.3 dB in Fig. 4(a). Aiming at investigating more details about the sound vibration at the location of 1023 m, we get the amplitude time-varying waveforms as shown in Fig. 4(b), which has large distortions in the sinusoidal shape. The frequency response is analyzed as shown in Fig. 4(c), and the 100 Hz frequency component can be seen in the spectrum. The single-point SNR is 10.8 dB, which is defined as power ratio between the signal frequency power and background noise frequency power.

Due to the relatively low SNR, the signal demodulation brings about some fake frequency components (the 160 Hz and 320 Hz), as shown in Fig. 4(c), which will greatly affect the

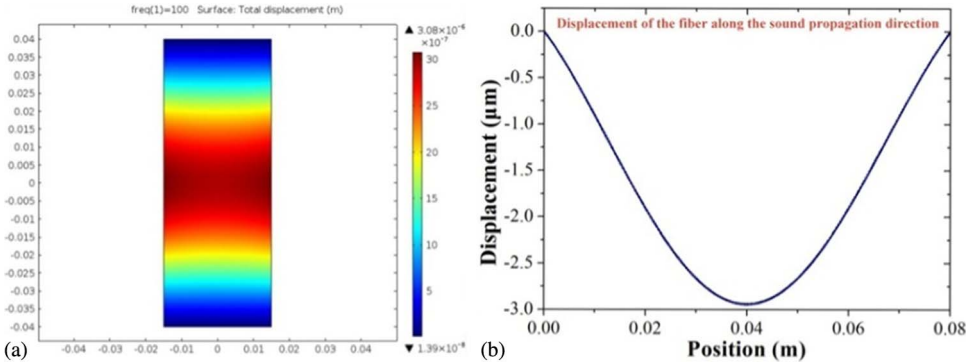

Fig. 5. Simulation result of the displacement of the flat-packaged setting under sound pressure. (a) Displacement distribution of the sheet metal along the sound propagation direction. (b) Displacement distribution of the fiber along the sound propagation direction.

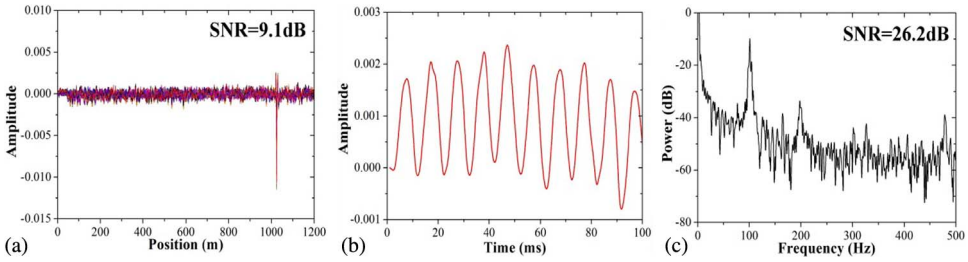

Fig. 6. Experimental result of the acoustic wave response based on the flat-packaged setting. (a) Distributed differential amplitude traces. (b) Differential amplitude time-varying waveforms at the vibration point. (c) Frequency spectrum of the amplitude waveforms.

accurate measurement. Because the fiber strain induced by acoustic wave is very slight, fiber loops have been designed and placed closing to the loud-speaker, which greatly enlarge the disturbed length (from 0.1 m to 5 m) and optical phase change. Based on this suspend-loop setting configuration, the differential amplitude trace detection scheme can basically achieve the sound wave capture and detection. However, this suspend-loop setting configuration is not convenient for the practical application.

In order to further improve the sensitivity of acoustic wave detection, the sensing fiber is pulled tightly and fixed with glue on the surface of a sheet metal (304 stainless steel) as illustrated in Fig. 3(b). The size of the sheet metal is 80 mm $\times$ 30 mm and the thickness is just 0.2 mm, the length of fiber fixed with the sheet metal is about 80 mm. When it is exposed to acoustic field, more energy of the acoustic wave will exert on metal sheet, which ultimately induces the larger deformation of fiber. In experiments, the loud-speaker with 7 cm diameter has been placed 5 cm in front of the metal sheet without any direct contact. The deformations of the sheet metal and fiber along the sound wave propagation direction are calculated by using simulation software (COMSOL Multiphysics), as shown in Fig. 5. The situation is set to be 100 Hz single frequency sound wave with 85 dBC sound pressure. Due to the fixed-ended boundary condition, the deformation of the sheet metal achieves maximum in the middle and decays gradually toward the edges as shown in Fig. 5(a). The fiber is glued and fixed in the middle of the sheet metal along the lengthwise direction. Therefore, the displacement of the fiber is just exactly the same with the corresponding bonded part of the sheet metal as shown in Fig. 5(b). The displacement of the fiber caused by the sound pressure can reach a few micrometers, and the vibration amplitude of the fiber has been enlarged greatly.

Based on this new flat-packaged setting, the experiment has been executed as the same with suspend-loop setting. As shown in the Fig. 6(a), the sound vibration location can be positioned

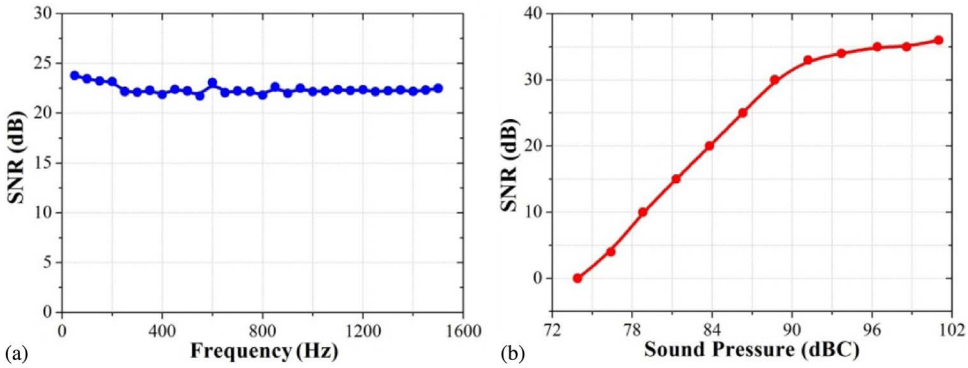

Fig. 7. Basic characteristics of the optical fiber microphone. (a) Frequency response curve, SNR versus sound frequency on the sensing fiber. (b) Intensity response curve, SNR versus sound pressure level on the sensing fiber.

easily at 1023 m. Compared with the suspend-loop setting configuration mentioned above, the global SNR in this case is greatly improved to be 9.1 dB, and the amplitude time-varying waveforms in Fig. 6(b) clearly show the detailed sinusoidal acoustic wave shape. The frequency response in Fig. 6(c) shows that the single-point SNR of flat-packaged setting has reached 26.2 dB, which is much higher than the suspend-loop setting and has little sign of fake-frequency components. Compared with 5 m length in the suspend-loop setting, we should note that here the effective length of flat-packaged setting is just 8 cm. Therefore, we adopt this flat-packaged differential amplitude demodulated φ-OTDR technique as the distributed optical fiber microphone scheme.

More details about the features of this distributed optical fiber microphone scheme have been investigated. Aimed at the human voice detecting and reproducing application, the frequency response curve has been obtain from the 50 Hz to 1.5 kHz as shown in Fig. 7(a). At all the sound frequency points, the sound pressure calibrated by standard electronic microphone has been set to be about 85 dBC. The frequency response is nearly flat for all frequencies with the single-point SNR fluctuated at the level of 22 dB. Also the sound pressure response has also been demonstrated at 100 Hz sinusoidal sound signal as shown in Fig. 7(b). The SNR decrease dramatically with sound pressure below the level of 76 dBC, and it is hard to distinguish the sound signal when the pressure is below 72 dBC. Here, we have to say that this SNR frequency response and the sensitivity is quite low compared with standard electronic microphone (~80 dB and 20 dBC, respectively), but this experiment has already realized the basic function of a preliminary optical fiber microphone.

To examine the multiplexing capability of this distributed optical fiber microphone, another experiment is conducted to simultaneously detect two sound vibrations with different frequencies at different locations. 100 Hz sinusoidal sound wave has been applied to the flat-packaged fiber section A at 1023 m position, and another 200 Hz sinusoidal sound wave has been applied to the flat-packaged fiber section B at 1100 m position. Both the applied sound pressures are set to be about 85 dBC. In order to avoid the overlap effect, the fiber length between section A and B should be larger than spatial resolution L (5 m in our experiment). Fig. 8(a) shows the experimental results of two sound vibrating simultaneously detection, which can be clearly identified that the sound vibrations are located at the positions of 1023 m and 1100 m, respectively. The differential amplitude time-varying waveforms and frequency spectrums at the positions A and B have been carefully investigated as shown in Fig. 8(b)–(e). The frequency responses and sensitivities of the multiple measurements are almost the same feature with the single point case as shown above. In particular, we could not see any identical frequency components of the two vibrations in the frequency spectrums of Fig. 8(c) and (e), which indicates that the sound wave at different positions can be demodulated independently with little crosstalk effect. However, due to the polarization and interferometer fade effect of the φ-OTDR system, the frequency responses and sensitivities of sound detection are not equal at all positions along the fiber. These

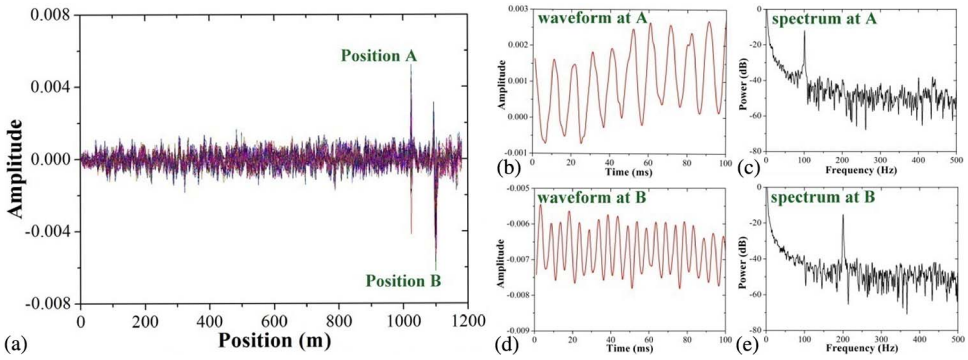

Fig. 8. Multiplexing capability of this distributed optical fiber microphone. (a) 100 consecutive superimposed traces of differential amplitude difference. (b) Differential amplitude time-varying waveforms at position A. (c) Frequency spectrum of the waveforms at position A. (d) Differential amplitude time-varying waveforms at position B. (e) Frequency spectrum of the waveforms at position B.

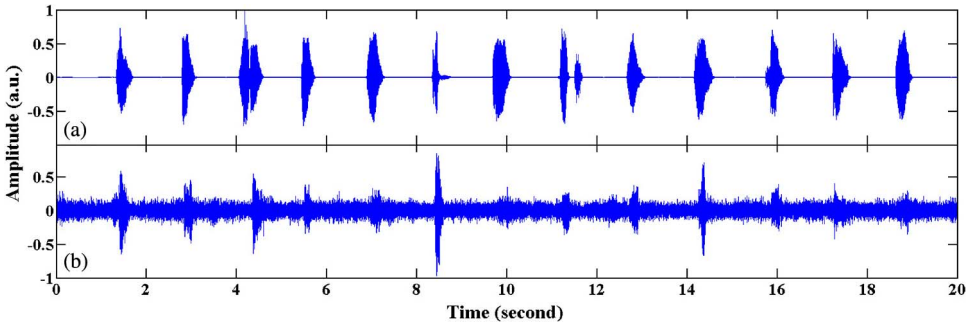

Fig. 9. Human voice demodulation capability of the distributed optical fiber microphone. (a) Audio waveform of the source. (b) Demodulated optical phase waveforms.

problems have been partly solved by using the polarization-maintaining optical sensing fiber and multi-frequency laser source [15], [16]. This is another scientific problem that needs to be taken into deep consideration.

Unlike the simulated single frequency sinusoidal sound wave used in above experiments, the real human voice is a complex signal, which is compose of acoustic waves of different frequencies and intensities, and changes rapidly with time. In order to investigate the complicated sound demodulation capability, an audio clip about the alphabet reading has been applied to the loud-speaker, and this audio has been tuned to be about 85 dBC in averaging pressure and broadcasted to a flat-packaged fiber section. Through the signal processing scheme of φ-OTDR system, we capture the broadcasting location at 1023 m and demodulate the waveforms of the differential amplitude difference induced by sound wave. Fig. 9(a) represents the audio waveforms of the source, which is an audio clip about the alphabet reading, and Fig. 9(b) shows the demodulated optical differential amplitude difference waveforms. Although there are a lot of differences in details, these two waveforms have roughly the same shapes and outlines, which indicates the successful sound reproduction. This demodulated optical differential amplitude waveform has been converted to be an audio file. Listening to the demodulation audio file, we can clearly recognize the alphabet reading information, although a lot of noises are mixed within the audio clip.

Because the change of fiber strain and phase induced by acoustic wave are still relatively slight, the sensitivity of our optical fiber microphone is relatively low and the single-point SNR can reach just about 35 dB, which is significantly lower than the practical human voice hearing application. Still, there are some methods to improve the SNR of this φ-OTDR system. First,

the Rayleigh scattering reinforced fiber can be used to enlarge the amount of the backward sensing related scattering light, such as the multimode fiber or large numerical aperture fiber. Secondly, we found the noises mainly origin from the laser source actually, so the frequency-stabilized narrow linewidth laser or the phase-locking between the source and local laser will seriously suppress the noise and improve the SNR.

3. Conclusion

Aimed at the human voice detecting and reproducing application, Rayleigh backscattering based φ-OTDR system has been proposed. In order to solve the ultra-low sensitivity of the φ-OTDR system for sound detection, the flat-packaged fiber sensor head design has been proved superior to suspend-loop design. Based on this flat-packaged φ-OTDR system, the frequency response and sensitivity have been investigated, also the multiplexing capability of this distributed optical fiber microphone have been proved. Human voice detection and reproduction experiments are successfully demonstrated, which indicates broad application prospects on acoustic wave detection.

References

[1] J. H. Cole, R. L. Johnson, and P. G. Bhuta, "Fiber optic detection of sound," *J. Acoust. Soc. Amer.*, vol. 62, no. 5, pp. 1136–1138, Nov. 1977.

[2] J. A. Bucaro, H. D. Dardy, and E. F. Carome, "Fiber optic hydrophone," *J. Acoust. Soc. Amer.*, vol. 62, no. 5, pp. 1302–1304, Nov. 1977.

[3] J. G. V. Teixeira, I. T. Leite, S. Silva, and O. Frazão, "Advanced fiber-optic acoustic sensors," *Photon. Sensors*, vol. 4, no. 5, pp. 198–208, Sep. 2014.

[4] Z. Fang, K. Chin, R. Qu, and H. Cai, *Fundamentals of Optical Fiber Sensors*. Hoboken, NJ, USA: Wiley, 2012, ch. 5.

[5] F. Guo *et al.*, "High-sensitivity, high-frequency extrinsic Fabry–Perot interferometric fiber-tip sensor based on a thin silver diaphragm," *Opt. Lett.*, vol. 37, no. 9, pp. 1505–1507, May 2012.

[6] N. Lagakos, T. R. Hickman, P. Ehrenfeuchter, J. A. Bucaro, and A. Dandridge, "Planar flexiblefiber-optic acoustic sensors," *J. Lightw. Technol.*, vol. 8, no. 9, pp. 1298–1303, Sep. 1990.

[7] M. Moccia *et al.*, "Opto-acoustic behavior of coated fiber Bragg gratings," *Opt. Exp.*, vol. 19, no. 20, pp. 18842–18860, Sep. 2011.

[8] S. W. Løvseth, J. T. Kringlebotn, E. Rønnekleiv, and K. Bløtekjær, "Fiber distributed-feedback lasers used as acoustic sensors in air," *Appl. Opt.*, vol. 38, no. 22, pp. 4821–4830, Aug. 1999.

[9] B. O. Guan, Y. N. Tan, and H. Y. Tam, "Dual polarization fiber grating laser hydrophone," *Opt. Exp.*, vol. 17, no. 22, pp. 19544–19550, Oct. 2009.

[10] A. Azmi *et al.*, "Fiber laser based hydrophone systems," *Photon. Sensors*, vol. 1, no. 3, pp. 210–221, Sep. 2011.

[11] F. Peng *et al.*, "Ultra-long high-sensitivity φ-OTDR for high spatial resolution intrusion detection of pipelines," *Opt. Exp.*, vol. 22, no. 11, pp. 13804–13810, Jun. 2014.

[12] Z. N. Wang *et al.*, "Phase-sensitive optical time-domain reflectometry with Brillouin amplification," *Opt. Lett.*, vol. 39, no. 15, pp. 4313–4316, Aug. 2014.

[13] Z. N. Wang *et al.*, "Ultra-long phase-sensitive OTDR with hybrid distributed amplification," *Opt. Lett.*, vol. 39, no. 20, pp. 5866–5869, Oct. 2014.

[14] Y. L. Lu, T. Zhu, L. A. Chen, and X. Y. Bao, "Distributed vibration sensor based on coherent detection of phase-OTDR," *J. Lightw. Technol.*, vol. 28, no. 22, pp. 3243–3249, Sep. 2010.

[15] Z. G. Qin, T. Zhu, L. Chen, and X. Y. Bao, "High sensitivity distributed vibration sensor based on polarization-maintaining configurations of phase-OTDR," *IEEE Photon. Technol. Lett.*, vol. 23, no. 15, pp. 1091–1093, May 2011.

[16] J. Zhou *et al.*, "Characteristics and explanations of interference fading of a OTDR with a multi-frequency source," *J. Lightw. Technol.*, vol. 31, no. 17, pp. 2947–2954, Jul. 2013.

[17] Q. He *et al.*, "Real distributed vibration sensing with high frequency response based on pulse pair," in *Proc. SPIE*, Santander, Spain, 2014, vol. 9157, p. 915761.

[18] T. Zhu, Q. He, X. Xiao, and X. Bao, "Modulated pulses based distributed vibration sensing with high frequency response and spatial resolution," *Opt. Exp.*, vol. 21, no. 3, pp. 2953–2963, Feb. 2013.

[19] Z. Pan *et al.*, "Phase-sensitive OTDR system based on digital coherent detection," in *Proc. SPIE*, 2011, vol. 8311, Art. ID 83110S.

[20] Z. Pan *et al.*, "Interference-fading-free phase-demodulated OTDR system," in *Proc. SPIE*, 2012, vol. 8421, Art. ID 842129.

[21] H. F. Taylor and C. E. Lee, "*Apparatus and method for fiber optic intrusion sensing*," U.S. Patent 5194847, Mar. 16, 1993.

[22] R. Posey, G. A. Johnson, and S. T. Vohra, "Strain sensing based on coherent Rayleigh scattering in an optical fibre," *Electron. Lett.*, vol. 36, no. 20, pp. 1688–1689, Sep. 2000.

[23] A. Masoudi, M. Belal, and T. P. Newson, "Distributed optical fibre dynamic strain sensor based on phase-OTDR," *Meas. Sci. Technol.*, vol. 24, no. 8, Jul. 2013, Art. ID 085204.

[24] F. Peng, Y. J. Rao, and Z. N. Wang, "Optical fiber distributed acoustic communication," presented at the Opt. Fiber Commun. Conf., Los Angeles, CA, USA, 2015, Paper W3I.6.
[25] M. Nakazawa, "Rayleigh backscattering theory for single-mode optical fibers," *J. Opt. Soc. Amer.*, vol. 73, no. 9, pp. 1175–1180, Apr. 1983.
[26] D. Subacius, A. Zavriyev, and A. Trifonov, "Backscattering limitation for fiber-optic quantum key distribution systems," *Appl. Phys. Lett.*, vol. 86, no. 1, Dec. 2005, Art. ID 011103.
[27] S. H. Xu *et al.*, "An efficient compact 300 mW narrow-linewidth single frequency fiber laser at 1.5 μm," *Opt. Exp.*, vol. 18, no. 2, pp. 1249–1254, Jan. 2010.